23 European Conference on Fracture - ECF23

Analysis of additively manufactured PLA containing notches using Failure Assessment Diagrams

Sergio Cicero[a]*, Víctor Martínez-Mata[a], Marcos Sánchez[a], Sergio Arrieta[a]

[a]LADICIM (Laboratorio de la División de Ciencia e Ingeniería de los Materiales), Universidad de Cantabria. E.T.S. de Ingenieros de Caminos, Canales y Puertos, Av. Los Castros 44, 39005 Santander, Spain

Abstract

This paper provides a methodology for the estimation of the load-bearing capacity of additively manufactured (AM) PLA specimens that may be applied to both cracked and notched conditions. The methodology is based on the use of Failure Assessment Diagrams (FADs), which are, in practice, the main fracture-plastic collapse assessment tool provided by structural integrity assessment procedures. When dealing with notch-type defects, the methodology requires, additionally, the application of a notch correction that it is based on the Theory of Critical Distances (TCD) and the Creager-Paris stress distribution ahead of the crack-tip. The results show that the FAD methodology (alone, in cracked conditions, or in combination with the TCD in notched conditions) can be successfully applied in this AM polymer.

1. Introduction

When dealing with structural failures in the presence of crack-like defects, assessment criteria are provided by structural integrity assessment procedures (e.g., FINTET FFS (Kocak et al. (2008) and Gutierrez-Solana and Cicero (2009)), BS7910 (2019), API 579‑1/ASME FFS‑1 (2016)), most of which are based on Failure Assessment

* Corresponding author. Tel.: +34-942-201705; fax: +34-942-201818.
  E-mail address: sergio.cicero@unican.es

Diagrams (FADs). These diagrams provide a simultaneous analysis of fracture and plastic collapse through two normalized parameters, Kr and Lr:

$$K_r = \frac{K_I}{K_{mat}} \tag{1}$$

$$L_r = \frac{P}{P_L} \tag{2}$$

where K_I is the stress intensity factor and K_{mat} is the material fracture resistance in terms of stress intensity factor units. Additionally, P is the applied load and P_L is the limit load. Consequently, K_r evaluates the (cracked) component against fracture, whereas L_r evaluates the (cracked) component against plastic collapse. K_r and L_r establish the coordinates of the resulting assessment point, which have to be compared with the critical conditions defined by the Failure Assessment Line (FAL): when the assessment point is located above the FAL, the component is considered to be under unsafe conditions, whereas if the assessment point is located within the area defined by the FAL and the coordinate axes, the component is considered to be under safe conditions. Lastly, the failure condition is defined when the assessment point lies exactly on the FAL, as defined in Kocak et al. (2008), Gutierrez-Solana and Cicero (2009), BS7910 (2019) and API 579‑1/ASME FFS‑1 (2016).

Nomenclature

AM	Additive manufacturing
E	Young´s modulus
e_{max}	Strain at maximum load
FAD	Failure Assessment Diagram
FAL	Failure Assessment Line
K_I	Stress intensity factor
K_{mat}	Fracture toughness
$K^N_{mat,avg}$	Average value of apparent fracture toughness
K^N_{mat}	Apparent fracture toughness
K_r	valuates the (cracked) component against fracture
L	Critical distance
L_r	valuates the (cracked) component against plastic collapse
P	Applied load
P_{est}	Critical load prediction
P_L	Limit load
P_{max}	Maximum load
$P_{max,avg}$	Average value of the maximum loads
PLA	Polylactic acid
SENB	Single edge notched bending specimens
TCD	Theory of Critical Distances
ρ	Notch radius
σ_y	Yield stress
σ_u	Tensile strength

In practice, there are situations where the defects that threaten the integrity of a given component or structure are not crack-like defects (e.g., mechanical damage, corrosion defects, fabrication defects, holes, corners, weld toes, etc.). When such defects are blunt, it may be overly conservative to proceed on the hypothesis that they behave like cracks and to apply fracture mechanics criteria. The literature reveals (e.g, Taylor (2007), Cicero et al. (2009), Cicero et al. (2011), Cicero et al. (2012), Madrazo et al. (2012), Cicero et al. (2013) and Cicero et al. (2014)) that components with non-sharp defects (i.e., notches) exhibit an apparent fracture toughness (K^N_{mat}) which is greater than that obtained in cracked conditions, and also that this may have an impact on the load-bearing capacity of the component being analyzed. The analysis of the fracture behavior of notched materials can be performed using different criteria (e.g.,

Taylor (2007), Hilleborg et al. (1976), Weibull (1939) and Sih (1974)), among which the Theory of Critical Distances (TCD) has been extensively explained and validated in Taylor (2007), and may be used to generate structural integrity assessment criteria for components containing notch-type defects, as proposed in Cicero et al. (2011) through the combination of FADs and the TCD.

Additionally, the aforementioned structural integrity assessment procedures address the analysis of metallic materials, but do not cover non-metallic materials which, on the other hand, are being incorporated into structural applications. Some research has provided FAD assessments of non-metallic materials containing cracks (e.g., Cicero et al. (2011) and Fuentes et al. (2018)) but, to the knowledge of the authors, there is no research analyzing the use of FADs in the assessment of 3D printed (fused deposition modelling) polymers. In this sense, additive manufacturing (AM), and particularly fused deposition modelling (FDM), is a growing technology that allows complex geometries to be generated using a relatively simple method, but the use of FDM materials in structural applications requires the development of specific structural integrity assessment criteria.

This work provides an approach to the structural integrity analysis of FDM PLA containing notches. With this aim, section 2 provides a description of the PLA material being analyzed, the tested specimens and the experimental and analytical procedures, section 3 gathers the results and the discussion, and section 4 outlines the main conclusions.

2. Materials and methods

60 fracture tests (SENB specimens, see Fig. 1) and 9 tensile tests were printed with the PLA material, considering three different raster orientations: 0/90, 30/-60 and 45/-45. Fracture specimens covered five different notch radii: 0 mm, 0,25 mm, 0,50 mm, 1 mm and 2 mm. The defects were machined, except for those whose notch radius was 0 mm (crack-like defects), which were produced by sawing using a razor blade.
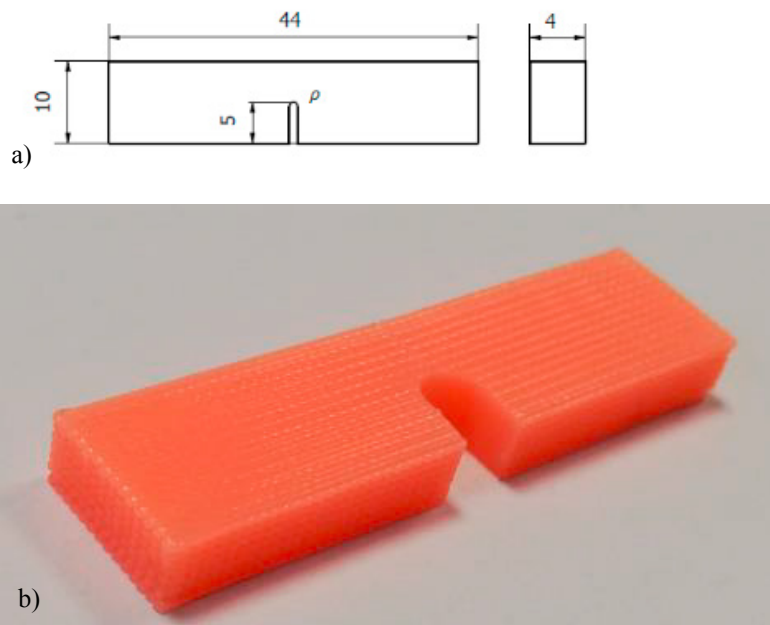

Fig. 1. PLA SENB specimens containing U-notches. a) Schematic of a generic specimen; b) image of a particular specimen, with notch radius (ρ) = 2.0 mm, and raster orientation 0/90.

All samples were manufactured by FDM with the following printing parameters: layer height 0.3 mm, nozzle diameter 0.4 mm, infill level 100%, printing temperature 200 ºC, bed temperature 75 ºC, and printing rate 30mm/s. Additional details may be found in Cicero et al. (2021).

Tensile tests were performed at room temperature following ASTM D638 (2014), whereas fracture tests were performed at room temperature following ASTM D5045 (2014) standard.

Concerning the assessment of the notched specimens, the procedure described in Cicero et al. (2011) was applied. It basically substitutes the real situation of a notched material whose fracture toughness is K_{mat}, by an equivalent situation of a cracked material whose fracture resistance is K^N_{mat} (material apparent fracture toughness for a given notch radius). Consequently, the notch correction may be introduced in the K_r parameter of the FAD:

$$K_r = \frac{K_I}{K^N_{mat}} \tag{3}$$

The value of K^N_{mat} is estimated using the notch correction derived from the combination of the TCD (Line Method by Taylor (2007)) and the Creager-Paris stress distribution ahead of a notch tip (Creager and Paris (1967)), leading to Cicero et al. (2011):

$$K_r = \frac{K_I}{K^N_{mat}} = \frac{K_I}{K_{mat}\sqrt{1+\frac{\rho}{4L}}} \tag{4}$$

where L is the critical distance, a material parameter that requires calibration (see Section 3).

Concerning the L_r parameter, the notch effect in the plastic collapse load is assumed to be negligible (Cicero et al. (2011) and Miller (1988)), and the P_L solutions derived for cracked conditions are used in notched conditions (i.e., L_r is the same as that used for cracks, equation (2), with available solutions in the literature for most of the practical situations). Regarding the FAL solutions to be used in the analysis of notches, it is possible to use the FALs proposed in structural integrity assessment procedures for the analysis of crack-like defects, given that the dependence of such solutions on the notch radius is very weak, as shown in Horn and Sherry (2012). Summarizing, the assessment of notches through Failure Assessment Diagrams only requires providing a correction of the material fracture resistance in the definition of the K_r parameter (e.g. equation (4)).

In this particular research, BS7910 Option 1 FAL was used in all cases, K_I solutions were taken from ASTM D5045 (2014), and P_L solutions were taken from Anderson (2005). Given that notched fracture specimens were in an intermediate situation between plane stress and plane strain conditions, the P_L used in the assessment was derived from the interpolation between the plane stress and plane strain solutions (e.g., Fuentes et al. (2018)).

3. Results and discussions

Table 1 gathers the tensile properties for the three raster orientations, with E being the Young´s modulus, σ_y being the yield stress, σ_u being the tensile strength and e_{max} being the strain under maximum load. The yield stress has been defined by the 0.2% offset strength, and the tensile strength has been defined by the maximum stress level of the corresponding curves. The results show that raster orientation 0/90 generates the highest tensile properties, and the lowest ductility. On the contrary, raster orientation 45/-45 provides the lowest tensile properties and the highest ductility.

Table 2 gathers the results of the fracture tests, together with the individual (P_{max}) and average values ($P_{max,avg}$) of the maximum loads. The conservatism of the approach is significant in most cases.

Table 1. Tensile properties per raster orientation (average and standard deviation), and L values derived from the best fitting of experimental fracture results derived from ASTM D5045.

	Raster orientation	E (MPa)	σ_y (MPa)	σ_u (MPa)	e_{max} (%)	L (mm)
	0/90	3769 ± 218	51,2 ± 0,9	52,0 ± 0,9	1,7± 0,2	0.57
PLA	30/-60	3313 ± 212	38,0 ± 3,7	42,0 ± 3,0	1,9± 0,1	0.38
	45/-45	2751 ± 406	35,3 ± 4,6	41,1 ± 5,7	2,6± 0,2	0.24

Table 2. Fracture toughness results on each individual test following ASTM D5045 standard, and experimental critical loads (P_{max}), and critical load predictions (P_{est}).

	Raster orientation	ρ (mm)	Test	P_{max} (N)	$P_{max,avg}$ (N)	K^N_{mat} (MPam$^{1/2}$)	$K^N_{mat,avg}$ (MPam$^{1/2}$)	Pest (N)
PLA	0/90	0.00	1	177.4		3.24		
		0.00	2	175.6	188.1	3.16	3.46	-
		0.00	3	204.2		3.95		
		0.00	4	195.4		3.48		
		0.25	1	238.0		4.64		
		0.25	2	217.9	230.3	4.39	4.55	161.0
		0.25	3	235.2		4.61		
		0.25	4	-		-		
		0.50	1	256.9		5.08		
		0.50	2	242.3	249.5	4.83	4.76	170.0
		0.50	3	249.4		4.37		
		0.50	4	-		-		
		1.00	1	266.2		4.53		
		1.00	2	287.6	268.5	4.73	5.01	178.0
		1.00	3	262.2		5.19		
		1.00	4	258.2		5.58		
		2.00	1	215.6		4.01		
		2.00	2	200.7	205.9	4.04	3.91	197.3
		2.00	3	211.4		3.79		
		2.00	4	196.1		3.80		
	30/-60	0.00	1	156.6		2.95		
		0.00	2	184.2	168.5	3.71	3.18	
		0.00	3	162.8		3.12		
		0.00	4	170.6		2.92		
		0.25	1	204.4		3.88		
		0.25	2	242.5	231.3	5.03	4.43	134.3
		0.25	3	247.2		4.36		
		0.25	4	-		-		
		0.50	1	250.9		5.04		
		0.50	2	240.7	242.1	4.46	4.81	136.5
		0.50	3	234.7		4.77		
		0.50	4	242.5		4.95		
		1.00	1	281.9		4.80		
		1.00	2	262.8	262.8	5.44	4.84	133.7
		1.00	3	257.5		4.51		
		1.00	4	249.3		4.60		
		2.00	1	213.5		4.22		
		2.00	2	204.9	209.6	3.32	3.88	148.7
		2.00	3	205.0		3.99		
		2.00	4	215.2		3.99		
	45/-45	0.00	1	148.6		2.89		
		0.00	2	135.2	147.2	2.50	2.82	
		0.00	3	138.6		2.74		
		0.00	4	166.8		3.13		
		0.25	1	238.8	246.0	4.66	4.75	117.3
		0.25	2	235.1		4.78		

0.25	3	266.6		5.23		
0.25	4	243.6		4.33		
0.50	1	241.6		4.88		
0.50	2	267.7	256.1	4.40	4.70	118.8
0.50	3	249.2		4.39		
0.50	4	265.9		5.13		
1.00	1	309.6		5.73		
1.00	2	289.4	286.8	5.19	5.08	110.0
1.00	3	284.8		4.89		
1.00	4	263.5		4.51		
2.00	1	196.0		3.64		
2.00	2	219.4	211.7	3.20	3.57	134.3
2.00	3	221.4		3.37		
2.00	4	210.1		4.08		

It can be observed that there is a clear notch effect in the three raster orientations, with (normally) higher fracture loads and fracture toughness values when the notch radius increases. However, unexpectedly, the fracture toughness values (and the fracture loads) are lower for a notch radius of 2.0 mm than for a notch radius of 1.0 mm.

The results obtained for the different notch radii allow the critical distance to be estimated for the different raster orientations. The fracture resistance results obtained for the different notch radii were graphically represented for each raster orientation, and L was obtained by fitting the denominator in equation (4) to the experimental results by using the least squares method. Fig. 2 shows an example of the fitting process, while Table 1 includes the different L values.
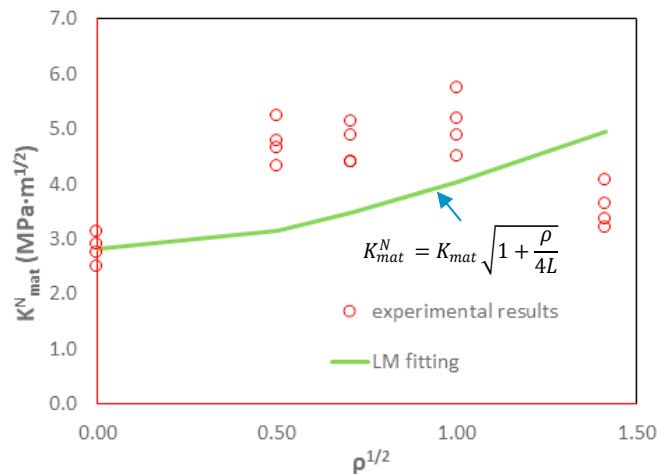

$$K_{mat}^{N} = K_{mat} \sqrt{1 + \frac{\rho}{4L}}$$

Fig. 2. Estimation of L from ASTM 5045 fracture results. 45/-45 raster orientation. L = 0.24 mm.

Once the tensile properties, the fracture properties, and L are known for each raster orientation, the FAD approach described above can be applied. When using equation (4), the value of K_{mat} considered here for each raster orientation is the corresponding average value obtained in cracked specimens (ρ = 0 mm). Fig. 3 shows the FAD assessment of the different notched specimens at fracture load, whereas Table 2 gathers the predictions of critical loads (P_{est}), which were obtained by determining the corresponding load that causes the assessment point to lie exactly on the FAL.
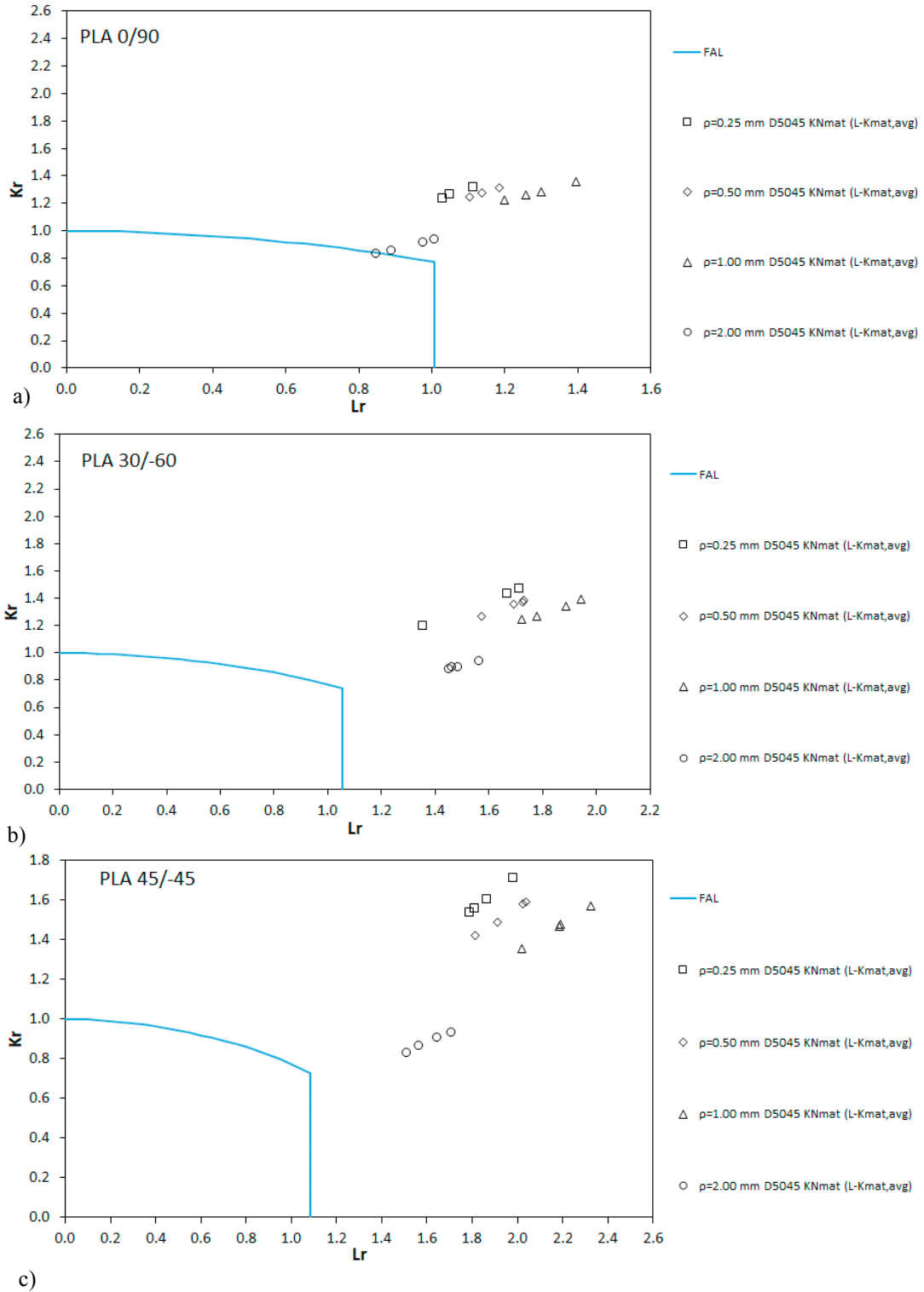
Fig. 3. FAD analysis of U-notched PLA specimens at failure. a) raster orientation 0/90; b) raster orientation 30/-60; raster orientation 45/-45.

The results show that the assessments provided when using ASTM D5045 average fracture toughness results are usually safe. Just one assessment point, in raster orientation 0/90, corresponds to an unsafe assessment in which the assessment point lies (slightly) below the FAL and P_{est} is a bit higher than P_{max}. The higher level of conservatism has been obtained in raster orientation 45/-45.

4. Conclusions

This paper proposes an approach for the assessment of U-notched additively manufactured polymers, and validates it by using experimental results obtained in additively manufactured PLA, with three different raster orientations. The approach assesses notched components by using Failure Assessment Diagrams in which the K_r parameter is defined as the ratio of the stress intensity factor to the apparent fracture toughness (K_I/K^N_{mat}). Additionally, K^N_{mat} is derived from the application of the Theory of Critical Distances.

The results obtained in this work show that the proposed approach usually provides safe results, with acceptable levels of conservatism when the FAD analysis is performed using average values of K_{mat}.

Acknowledgements

References

Anderson, T.L., 2005. Fracture mechanics: fundamentals and applications. 4th ed. Boca Raton: CRC Press - Taylor and Francis Group.

API RP 579-1 / ASME FFS-1, 2016. "API 579-1/ASME FFS-1, Third edition". The American Society of Mechanical Engineers, New York, USA.

ASTM D5045-14, 2014. Standard Test Methods for Plane-Strain Fracture Toughness and Strain Energy Release Rate of Plastic Materials, ASTM International, West Conshohocken, PA.

ASTM D638-14, 2014. Standard Test Method for Tensile Properties of Plastics. West Conshohocken, PA: ASTM International.

BS 7910:2019, 2019. "Guide to methods for assessing the acceptability of flaws in metallic structures". British Standard Institution, London, UK.

Cicero, S., Gutierrez-Solana, F., and Horn, A.J., 2009. Experimental analysis of differences in mechanical behaviour of cracked and notched specimens in a ferritic-pearlitic steel: Considerations about the notch effect on structural integrity, Eng. Fail. Anal., 16, 2450- 2466.

Cicero, S., Madrazo V. and Carrascal, I.A. and Cicero, R., 2011. Assessment of notched structural components using failure assessment diagrams and the theory of critical distances, Eng. Fract. Mech., 78, 2809-2825.

Cicero, S., Madrazo V. and Carrascal, I.A., 2012. Analysis of notch effect in PMMA by using the theory of critical distances, Eng. Fract. Mech., 86, 56-72.

Cicero, S., Madrazo V., García, T., Cuervo, J. and Ruiz, E., 2013. On the notch effect in load bearing capacity, apparent fracture toughness and fracture mechanisms of polymer PMMA, aluminium alloy Al7075-T651 and structural steels S275JR and S355J2, Eng. Fail. Anal., 29, 108- 121.

Cicero, S., Madrazo V. and García, T., 2014. Analysis of notch effect in the apparent fracture toughness and the fracture micromechanisms of ferritic-pearlitic steels operating within their lower shelf, Eng. Fail. Anal., 36, 322- 342.

Cicero, S., Martínez-Mata, V., Castanon-Jano, L., Alonso-Estebanez, A., and Arroyo, B., 2021. Analysis of notch effect in the fracture behaviour of additively manufactured PLA and graphene reinforced PLA, Theoretical and Applied Fracture Mechanics 114, 103032

Creager, M. and Paris, P.C., 1967. Elastic field equations for blunt cracks with reference to stress corrosion cracking, Int. J. Fract.Mech. 3, 247–252.

Fuentes, J.D., Cicero, S., Ibáñez-Gutiérrez, F.T. and Procopio, I., 2018. "On the use of British standard 7910 option 1 failure assessment diagram to non-metallic materials". Fatigue and Fracture of Engineering Materials and Structures Vol. 41: pp. 146–158.

Gutiérrez-Solana, F. and Cicero, S., 2009. "FITNET FFS Procedure: A unified European procedure for structural integrity assessment". Engineering Failure Analysis Vol. 16: pp. 559-577. https://doi.org/10.1016/j.engfailanal.2008.02.007

Hilleborg, A., Modeer, M. and Petersson, P.E., 1976. Analysis of crack formation and crack growth in concrete by means of fracture mechanics and finite elements, Cem. Concr. Res. 6, 777–782.

Horn, A.J., and Sherry, A.H., 2012. An engineering assessment methodology for non-sharp defects in steel structures - Part I: procedure development, Int. J. Press. Vessel. Pip. 89, 137–150.

Kocak, M., Webster, S., Janosch J.J., Ainsworth, R.A. and Koers, R., 2008. FITNET fitness-for-service (FFS), procedure, Vol. 1, GKSS Hamburg, Germany.

Madrazo, V., Cicero, S., and Carrascal, I.A., 2012. On the point method and the line method notch effect predictions in Al7075-T651, Eng. Fract. Mech., 79, 363-379.

Miller, A.G., 1988, Review of limit loads of structures containing defects, International Journal of Pressure Vessels and Piping, 32, 197-327.

Sih, G.C., 1974. Strain-energy-density factor applied to mixed mode crack problems, Int. J. Fract. 10, 305–321.

Taylor, D., 2007. The theory of critical distances: a new perspective in fracture mechanics, Elsevier, UK.

Weibull, W., 1939. The phenomenon of rupture in solids, Proc. R. Swed. Inst. Eng. Res. 153, 1–55.